Optimal Energy Trajectory Generation Based on Pitch-Dependent Mutual Inductance Model for In-Flight Inductive Power Transfer of Drones

Kota Fujimoto[1], Hiroshi Fujimoto[2]
The University of Tokyo
Kashiwa, Chiba, Japan
fujimoto.kota21@ae.k.u-tokyo.ac.jp[1], fujimoto@k.u-tokyo.ac.jp[2]

Alessandro Correa Victorino[3], Pedro Castillo[4]
Université de technologie de Compiègne, CNRS,
Heudiasyc (Heuristics and Diagnosis of Complex Systems)
Compiegne, France
(acorreav[3], castillo[4])@hds.utc.fr

***Abstract*—To address the challenge of limited flight duration in drones, research into in-flight inductive power transfer has emerged as a crucial solution. In this regard, optimizing the flight trajectory is vital for maximizing energy reception during a single pass over the transfer coils. This paper proposes a strategy that incorporates trajectories optimized on the basis of pitch angle. The optimal trajectories are derived analytically using a pitch-dependent mutual inductance model, and implemented on the drone's motion controller as the reference input for each cascaded control loop. The proposed method has been validated through simulations and experiments. Implementation of two proposed trajectories in the experiments reveals that the drone's receiving power can be improved by 13.4 % maximum compared to the conventional method.**

***Index Terms*—trajectory generation, pitch-dependent mutual inductance model, in-flight inductive power transfer**

I. Introduction

Drones are increasingly being used in various sectors of human society. Their application often requires operation along fixed routes. One typical example is security surveillance, as illustrated in Fig. 1. In this scenario, frequent battery charging is necessary, reducing the drone's operational efficiency. To enhance the efficiency, inductive power transfer (IPT) for drones, as suggested in [1], [2], is proposed for fixed-route operations, as also shown in Fig. 1.

This system, however, faces challenges in maintaining constant power and high efficiency, as drones may fluctuate in their path near the transmitter coils. Previous studies have achieved constant power transfer by controlling the converters [3] or driver coil [4], but they assume mutual inductance fluctuations and do not focus on efficiency improvement through optimal trajectories in regards of the motion control.

Prior research on optimal trajectories for dynamic wireless power transfer (DWPT) systems primarily concentrated on minimizing deviation perpendicular to the forward direction by first estimating the deviation [5], [6], and then controlling the lateral position [7], [8]. These studies, however, do not account for drones' ability to change altitude and angles, which is possible in the in-flight IPT system.

Rapid altitude and angle changes to follow optimal trajectories require the implementation of advanced controllers.

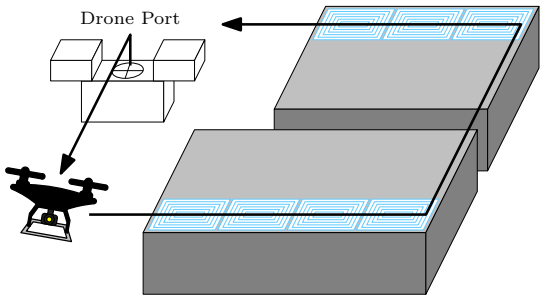

Fig. 1. Security mission with in-flight inductive power transfer system.

While some studies adopt a feedback approach [9]–[11], its effectiveness is limited by sensor characteristics, necessitating the use of a feedforward (FF) controller [12], [13]. There has been extensive research on FF control for drones [14], [15]. Shin et al. [14] proposed a neural-network-based FF controller, which requires the determination of numerous parameters. Chu et al. [15] introduced an adaptive FF controller characterized by multiple parameters and a complex control structure.

Against this backdrop, after the problem formulation in section Ⅱ, we propose optimal trajectories for efficient in-flight IPT in section Ⅲ. Reference trajectories are created for each cascaded loop in the drone's control system, including the position control loop and pitch angle control loop. This approach is equivalent to simply adding FF input for the pitch angle control loop. The trajectories are analytically derived based on the optimal pitch angle for each position above the transfer coil. The possibility of energy enhancement based on the proposed method is verified through the simulations and experiments in section Ⅳ and Ⅴ.

II. Problem formulation

A. Model of inductive power transfer system for input power calculation

In this part, we derive the theoretical formulas for the IPT circuit as shown in Fig. 2. Regarding Fig. 2, v_1, v_2, i_1, i_2 are transfer-side voltage, receiver-side voltage, transfer-side current, and receiver-side current, respectively. R_1, R_2,

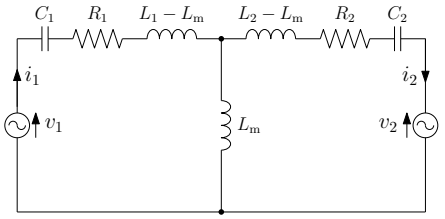

Fig. 2. Equivalent circuit of inductive power transfer system.

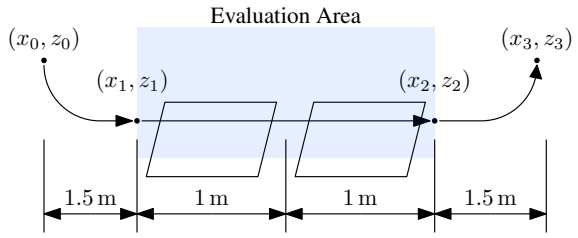

Fig. 3. Trajectory diagram of in-flight inductive power transfer system.

C_1, C_2, L_1, L_2, L_m are transfer-side resistance, receiver-side resistance, transfer-side capacitance, receiver-side capacitance, transfer-side inductance, receiver-side inductance, and mutual inductance, respectively.

From [16], the optimal transmission efficiency at the resonance condition η_{opt} is calculated as,

$$\eta_{\mathrm{opt}} = \frac{\left(\omega_0 L_m\left(x,y,z,\theta\right)\right)^2}{\left\{\sqrt{R_1 R_2} + \sqrt{R_1 R_2 + \left(\omega_0 L_m\left(x,y,z,\theta\right)\right)^2}\right\}^2}. \quad (1)$$

L_m can be calculated based on the position (x, y, z) and pitch angle θ from [17]. Finally, the input energy for the battery E_{in} is calculated as,

$$\begin{aligned} E_{\mathrm{in}}\left(x,y,z,\theta\right) &= \int_0^T P_1 \eta_{\mathrm{opt}}\left(x,y,z,\theta\right)\eta_{\mathrm{rect}}\mathrm{d}t, \\ &= \eta_{\mathrm{rect}} P_1 \int_0^T \eta_{\mathrm{opt}}\left(x,y,z,\theta\right)\mathrm{d}t, \end{aligned} \quad (2a)$$

where η_{rect}, P_1, T are the efficiency of the rectifier, transmission power form the transfer coil, time span in the evaluation area, respectively. In this study, P_1 is set as a constant for the sake of simplicity.

B. Energy consumption model of drone for output power calculation

In this part, the energy consumption model of the drone is presented. The output energy E_{out} is calculated as below:

$$E_{\mathrm{out}} = \frac{1}{\eta_{\mathrm{inv}}\eta_m\eta_p}\sum_{i=1}^{N}\left(\frac{1}{2}m\boldsymbol{v}^2 + \frac{1}{2}\boldsymbol{J}\boldsymbol{\omega}^2\right) + \frac{z[N]-z[1]}{\eta_{\mathrm{inv}}\eta_m\eta_p}, \quad (3)$$

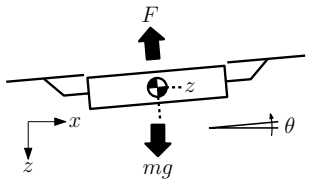

Fig. 4. Drone model.

where,

$$\boldsymbol{v} = \begin{bmatrix} v_x & v_y & v_z \end{bmatrix}^\top, \quad (4a)$$

$$\boldsymbol{\omega} = \begin{bmatrix} w_{\mathrm{roll}} & w_{\mathrm{pitch}} & w_{\mathrm{yaw}} \end{bmatrix}^\top, \quad (4b)$$

$$\boldsymbol{J} = \begin{bmatrix} J_{\mathrm{roll}} & 0 & 0 \\ 0 & J_{\mathrm{pitch}} & 0 \\ 0 & 0 & J_{\mathrm{yaw}} \end{bmatrix}. \quad (4c)$$

Here, m, J_{roll} , J_{pitch} , J_{yaw} are the mass and inertia for the roll, pitch, and yaw direction, respectively. z, v_x, v_y, v_z, w_{roll} , w_{pitch} , w_{yaw} are the altitude, velocity for x, y, z direction, and angular velocity for the roll, pitch, yaw direction, respectively. η_{inv}, η_{m}, η_{p}, and N are the efficiency of the inverter, motor, propeller, and number of the data sampled from the start point, respectively.

C. Problem formulation regarding received energy for single passing above transfer coil by drone

The performance of the designed trajectory and controller is determined by how effectively drones can receive the energy during a single flying above the transfer coil. Fig. 3 illustrates the trajectory diagram of the in-flight IPT system. The drone goes through from (x_0, z_0) to (x_3, z_3), and receives power from the transfer coils in the section between (x_1, z_1) and (x_2, z_2), which is termed as "evaluation area" in this research.

Within this framework, our goal is to maximize the energy received within the evaluation area during a single passing. To fairly evaluate each trajectory and controller, the time duration for the single fly is fixed as a constant. To realize the efficient IPT system, it is assumed that energy is transferred from the transfer coil when the transmission efficiency, denoted as η_{opt}, surpasses the threshold efficiency η_0. Given these conditions, the maximization problem of the receiving energy E_L is defined as follows based on (2) and (3):

$$\exists x(t), \exists \theta(t), \mathrm{max}.E_L = E_{\mathrm{in}} - E_{\mathrm{out}}, \quad (5)$$

where,

$$v_{x,\mathrm{ave}} = \int_0^T v_x(t)\mathrm{d}t = \mathrm{const.}, \quad (6a)$$

$$\eta = \begin{cases} \frac{\left(\omega_0 L_m(x,y,z,\theta)\right)^2}{\left\{\sqrt{R_1R_2}+\sqrt{R_1R_2+\left(\omega_0 L_m(x,y,z,\theta)\right)^2}\right\}^2}, & \text{if } \eta > \eta_0, \\ 0, & \text{otherwise.} \end{cases} \quad (6b)$$

D. Drone motion model on plane

Fig. 4 illustrates the schematics of the drone within x–z plane. The motion equation for the depicted model in Fig. 4

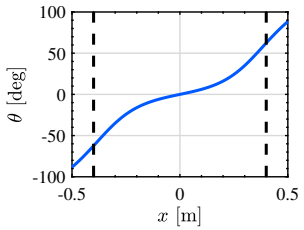

Fig. 5. Optimal pitch angle at each position above one transfer coil.

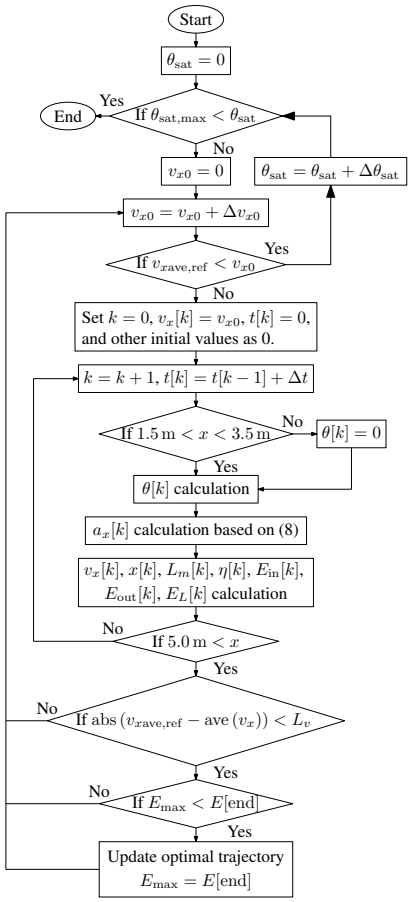

Fig. 6. Flowchart of trajectory design algorithm.

can be expressed as:

$$m\ddot{x} = -F\sin\theta, \tag{7a}$$

$$m\ddot{z} = mg - F\cos\theta, \tag{7b}$$

$$J_{\text{pitch}}\ddot{\theta} = \tau_{\text{pitch}}. \tag{7c}$$

Here, g, F, and τ_{pitch} are the gravitational constant, total thrust, and total torque for the pitch direction, respectively. Given that drones maintain a consistent altitude when flying over the transfer coil, we can set $\ddot{z} = 0$. Thus, based on (7), the subsequent equation is formulated:

$$\ddot{x} = -g\tan\theta. \tag{8}$$

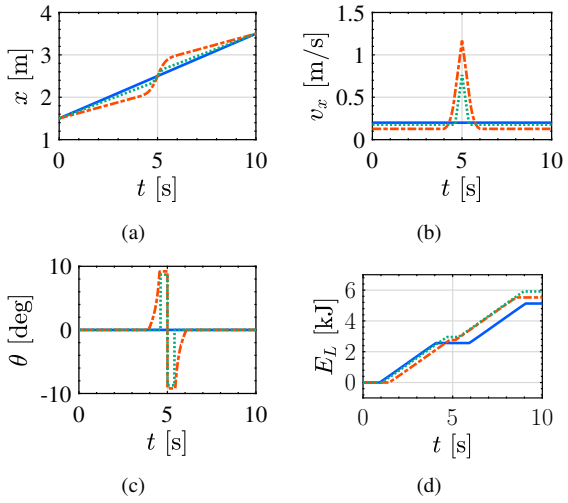

Fig. 7. Designed trajectory. Straight trajectory (——), optimal pitch trajectory (- - -), and edge pitch trajectory (· · · ·). (a) Position x (b) Velocity v_x (c) Pitch angle θ (d) Receiving energy E_L

TABLE I
SYSTEM PARAMETERS.

Parameter	Value
Mass m	1.2 kg
Roll inertia J_{roll}	0.006 kg m^2
Pitch inertia J_{pitch}	0.006 kg m^2
Yaw inertia J_{yaw}	0.1 kg m^2
Arm length l	0.2 m
Transfer-side resistance R_1	200 mΩ
Receiver-side resistance R_2	50 mΩ
Operational frequency ω_0	85 kHz
Primary Power P_1	1 kW
Inverter efficiency η_{inv}	0.95
Motor efficiency η_m	0.90
Propeller efficiency η_p	0.90
Rectifier efficiency η_{rect}	0.95
Threshold efficiency η_0	0.80
Reference average velocity $v_{x\text{ave,ref}}$	0.20 m/s
Maximum pitch angle saturation $\theta_{\text{sat,max}}$	10.0 deg
Error threshold of average velocity L_v	10^{-4} m/s

III. OPTIMAL TRAJECTORY DESIGN

A. Optimal pitch angle at each position above transfer coil

First, the optimal pitch angle at each position above the transfer coil is analyzed. As shown in Fig. 3, we assume the single coil area as 1 m, where the transfer coil with the length of 0.8 m is located at the center of the area. The drone's position is fixed at $y = 0$ m and $z = 0.2$ m, with the assumption that both of the drone's roll angle φ and yaw angle ψ are maintained at 0 deg. Under these conditions, the optimal

TABLE II
DESIGNED PARAMETERS.

	v_{x0} [m/s]	θ_{sat} [deg]	Total E [kJ]	Improved Rate [%]
Straight	0.20	0.0	5.12	0
Optimal pitch	0.127	9.20	5.52	7.81
Edge pitch	0.177	8.70	5.92	15.6

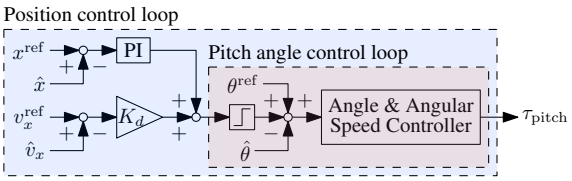

Fig. 8. Block diagram of drone position controller on x axis.

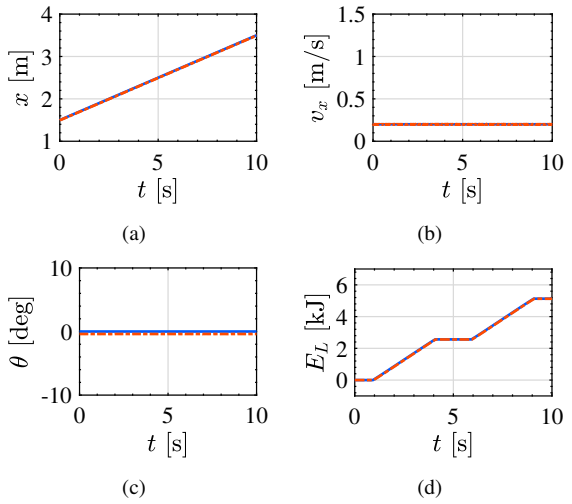

Fig. 9. Simulation results of straight trajectory. Reference value (—) and measured value (- - -). (a) Position x (b) Velocity v_x (c) Pitch angle θ (d) Receiving energy E_L

pitch angle θ, which maximizes transmission efficiency as shown in (1), is computed by varying θ within the range $(-90\,\text{deg}, 90\,\text{deg})$. The calculation results based on the system parameters as listed in Table. I are shown in Fig. 5.

B. Trajectory design based on optimal pitch

This part describes the trajectory design algorithm. We propose two trajectories for the energy maximization, including the conventional "straight trajectory" with the constant velocity. The first, termed the "optimal pitch trajectory," is characterized by selecting the analytically optimal pitch angle over all the regions between the central points of adjacent coils as the reference values. The second, termed "edge pitch trajectory," is characterized by adopting the optimal pitch angle only when the computed transmission efficiency, using (1), falls below the threshold η_0. This approach results in a larger pitch angle only at the edges of the transfer coils.

Fig. 6 presents the flowchart for the trajectory design algorithm. Initially, the drone is positioned at (x_0, z_0), with

TABLE III
SIMULATION RESULTS.

	Total Time [s]	Total Energy [kJ]	Improved Rate [%]
Straight	10.0	5.12 (5.12)	0 (0)
Optimal pitch	10.0	5.48 (5.48)	7.03 (7.03)
Edge pitch	10.0	5.70 (5.70)	11.3 (11.3)

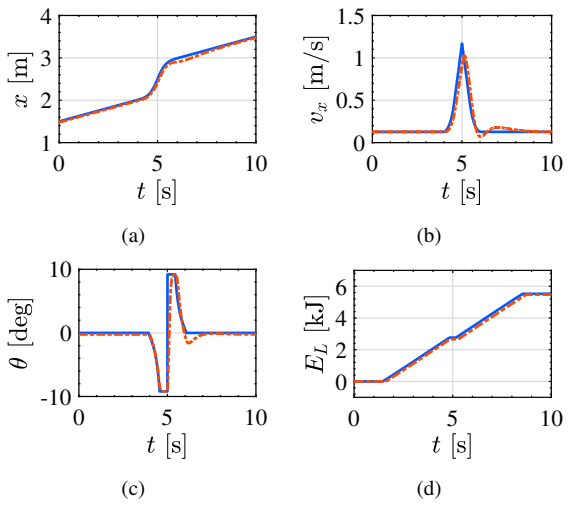

Fig. 10. Simulation results of optimal pitch trajectory. Reference value (—) and measured value (- - -). (a) Position x (b) Velocity v_x (c) Pitch angle θ (d) Receiving energy E_L

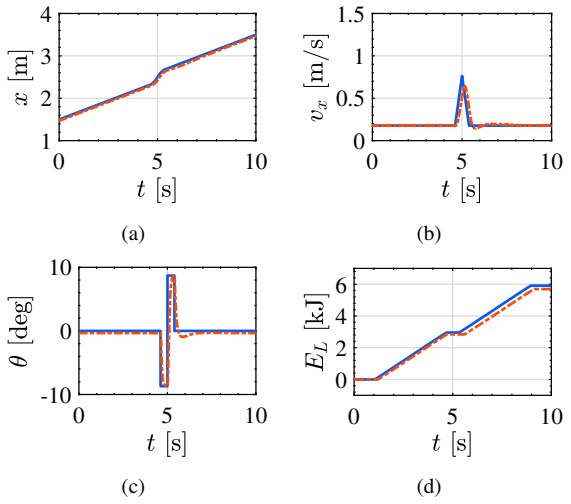

Fig. 11. Simulation results of edge pitch trajectory. Reference value (—), and measured value (- - -). (a) Position x (b) Velocity v_x (c) Pitch angle θ (d) Receiving energy E_L

a minimum initial velocity $v_{x0} = \Delta v_{x0}$ and pitch angle saturation $\theta_{\text{sat}} = 0\,\text{deg}$ The initial velocity v_{x0} is chosen to be the same with or less than the reference average velocity within the evaluation area, denoted $v_{x\text{ave,ref}}$. The pitch angle saturation θ_{sat} is also optimized with the maximum value $\theta_{\text{sat,max}}$.

When x lies between $1.5\,\text{m}$ and $3.5\,\text{m}$, θ calculations are performed for each trajectory. Subsequently, the full trajectory parameters are derived by calculating the acceleration $a_x[k] = \ddot{x}[k]$ and other variables such as $v_x[k]$, $x[k]$, $L_m[k]$, $\eta[k]$, $E_{\text{in}}[k]$, $E_{\text{out}}[k]$, and $E_L[k]$, by referring the equations detailed in the section II. The process finishes when $x[k] > 5.0\,\text{m}$. If the absolute difference between $v_{x\text{ave,ref}}$ and the average velocity $\text{ave}\,(v_x)$ is less than the threshold L_v, and the total energy $E[\text{end}]$ exceeds the recorded maximum energy $E_{\max}$,

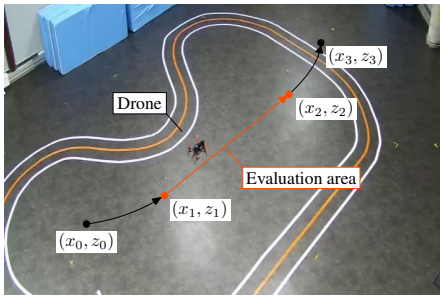

Fig. 12. Experimental setups.

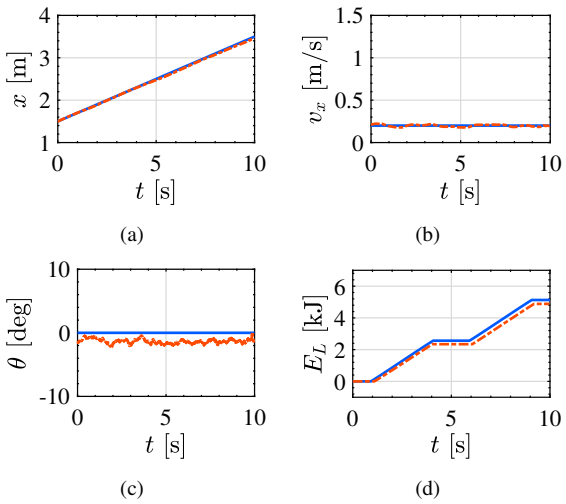

Fig. 13. Experimental results of straight trajectory. Reference value (—) and measured value (- - -). (a) Position x (b) Velocity v_x (c) Pitch angle θ (d) Receiving energy E_L

the optimal trajectories are updated and the iterations continue.

Fig. 7 depicts the optimized trajectories. The designed parameters are shown in Table. II. As shown in Fig. 7, the optimal pitch trajectory can improve the receiving energy by 7.81 % compared to the conventional method. Conversely, the edge pitch trajectory can improve the receiving energy by 15.6 %. Each designed trajectory is implemented as x^{ref}, v_x^{ref}, and θ^{ref} shown in Fig. 8.

IV. Simulations

The simulations are carried out to validate the proposed method. These simulations are executed within FL-AIR, the drone simulation software developed in C++, where we can simulate the nonlinear drone system. The proposed system, including the trajectories from Fig. 7 and the controller from Fig. 8, is integrated into this simulator.

The simulation results are shown in Figs. 9-11, focusing on only the evaluation area. Table. III shows the total time in the evaluation area, total receiving energy by drones, and improved rate of energy compared to the straight trajectory. The compensated values of the total energy and improved rate based on the total time are shown in parentheses. The values are linearly compensated in case drones remain in the evaluation area beyond the scheduled time span.

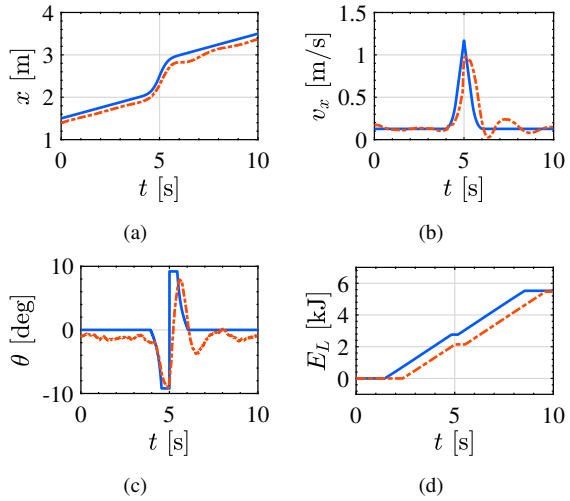

Fig. 14. Experimental results of optimal pitch trajectory. Reference value (—) and measured value (- - -). (a) Position x (b) Velocity v_x (c) Pitch angle θ (d) Receiving energy E_L

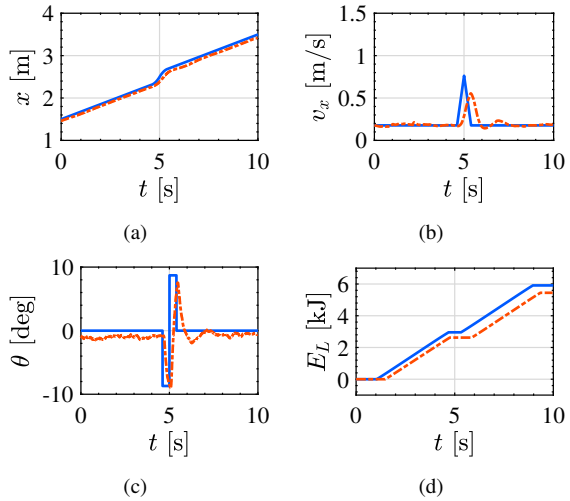

Fig. 15. Experimental results of edge pitch trajectory. Reference value (—) and measured value (- - -). (a) Position x (b) Velocity v_x (c) Pitch angle θ (d) Receiving energy E_L

Fig. 9 illustrates the results for the straight trajectory, which is referred to as the benchmark. Fig. 10 shows the results for the optimal pitch trajectory, indicating the enhanced total energy by 7.03 % compared to the conventional method. Fig. 11 presents the results for the edge pitch trajectory, where the total energy can be improved by 11.3 %. These results suggest that the proposed trajectory can be effective for the in-flight IPT system to receive more energy in the constant time span. Additionally, it is observed that the edge pitch trajectory can accomplish higher energy than the optimal pitch trajectory on the ideal situation created in the simulator.

V. Experiments

The experiments are conducted to evaluate the performance of our proposed trajectory in the real world. For these experiments, we utilize the AR Drone 2, depicted in Fig. 12.

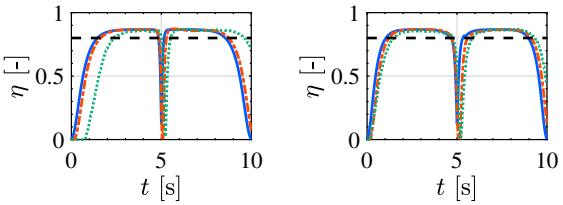

Fig. 16. Transmission efficiency in proposed trajectory. Designed value (—), simulation value (-·-), and experimental value (····). (a) Optimal pitch trajectory (b) Edge pitch trajectory

TABLE IV
EXPERIMENTAL RESULTS

	Total Time [s]	Total Energy [kJ]	Improved Rate [%]
Straight	10.2	4.88 (4.78)	0 (0)
Optimal pitch	10.1	5.48 (5.42)	12.3 (13.4)
Edge pitch	10.2	5.44 (5.34)	11.5 (11.7)

The position and velocity are measured with OptiTruck and incorporated into the control system. The receiving energy is also calculated by (5) based on the measured values.

The experimental results are shown in Figs. 13-15 and Table. IV. Fig. 13 depicts the results for the straight trajectory, which is functioned as the conventional trajectory. Fig. 14 shows the results of the optimal pitch trajectory. As shown in Table. IV, the total energy can be improved by $13.4\,\%$ compared to the conventional method. Fig. 15 shows the results of the edge pitch trajectory. This trajectory shows an improved total energy by $11.7\,\%$, which is worse than the optimal pitch trajectory.

This seems to be because the experimental results of the optimal pitch trajectory have the quick position response just after $5\,\mathrm{s}$, when changing the pitch angle rapidly, though it has a late position response in general. Fig. 16 shows the time responses of transmission efficiencies based on the optimal pitch trajectory and edge pitch trajectory. When each line is above the black line, drones can receive the power. In Fig. 16(a), just after $0\,\mathrm{s}$ and $8\,\mathrm{s}$, the transmission efficiency η has the late response for the designed value. On the other hand, just after $5\,\mathrm{s}$ in Fig. 16(a), it has a quick response, though such kind of response speed changes do not happen on the edge pitch trajectory. Thanks to that, drones can receive more power in the latter half of the evaluation area, which leads to higher energy receiving at the final state.

These experimental results show the effectiveness of our proposed method for enhancing the calculated performance of the in-flight IPT system. The improvement of the trajectory response will be scrutinized in future studies.

VI. CONCLUSION

In this study, we introduce an optimal trajectory to improve the receiving energy. The effectiveness of our approach is examined through the simulations and the experiments. Experimental results show the $13.4\,\%$ enhancement of the total calculated energy with the optimal pitch trajectory and the $11.7\,\%$ enhancement with the edge pitch trajectory in in-flight IPT system.

In future studies, we will elaborate on the problem formulation, incorporating constraints such as the maximum velocity and acceleration which seem to be relevant to motor abilities. Additionally, we will engage in the advanced motion controller design for the fast transient controller in order to obtain a uniform response when implementing the proposed trajectories. Finally, the proposed trajectories and controllers will be applied in the actual in-flight IPT system.

ACKNOWLEDGEMENT

This work has been funded in part by the European OWHEEL project grant n°872907, and UTC SFRi fellowship program. This work was also partly supported by JSPS KAKENHI Grant Number JP23H00175, Japan.

REFERENCES

[1] K. Chen and Z. Zhang, "In-Flight Wireless Charging: A Promising Application-Oriented Charging Technique for Drones," *IEEE Industrial Electronics Magazine (Early Access)*, pp. 2–12, 2023.

[2] J. M. Arteaga, S. Aldhaher, G. Kkelis, C. Kwan, D. C. Yates, and P. D. Mitcheson, "Dynamic Capabilities of Multi-MHz Inductive Power Transfer Systems Demonstrated With Batteryless Drones," *IEEE Transactions on Power Electronics*, vol. 34, no. 6, pp. 5093–5104, 2019.

[3] Z. Zhang, S. Shen, Z. Liang, S. H. K. Eder, and R. Kennel, "Dynamic-Balancing Robust Current Control for Wireless Drone-in-Flight Charging," *IEEE Transactions on Power Electronics*, vol. 37, no. 3, pp. 3626–3635, 2022.

[4] T. Ohori, X. Li, H. Nakanishi, S. Ozawa, and W. Hijikata, "Wireless Power Transfer System for Mobile Robots with Impedance Matching by Adjusting Position of Driver Coil," *IEEJ Journal of Industry Applications*, vol. 12, no. 5, pp. 945–952, 2023.

[5] P. Sukprasert, B. M. Nguyen, and H. Fujimoto, "Estimation and Control of Lateral Displacement of Electric Vehicle Using WPT Information," in *IEEE International Conference on Mechatronics (ICM)*, 2015.

[6] T. Koishi, R. Matsumoto, and H. Fujimoto, "Estimation and Positioning Control of Lateral Displacement Using Coil Current in Dynamic Wireless Power Transfer with Rectangular Coil on Dynamic Bench," in *IEEE Wireless Power Week (WPW)*, 2022.

[7] Z. Lu, B. Shyrokau, B. Boulkroune, S. van Aalst, and R. Happee, "Performance Benchmark of state-of-the-art Lateral Path-following Controllers," in *IEEE 15th International Workshop on Advanced Motion Control (AMC)*, 2018.

[8] T. Enmei, H. Fujimoto, and V. Ivanov, "Proposal of Lateral Force Disturbance Estimation Method for In-Wheel-Motored Electric Vehicles," in *The 44th Annual Conference of the IEEE Industrial Electronics Society (IECON)*, 2018.

[9] A. Castillo, R. Sanz, P. Garcia, W. Qiu, H. Wang, and C. Xu, "Disturbance observer-based quadrotor attitude tracking control for aggressive maneuvers," *Control Engineering Practice*, vol. 82, pp. 14–23, 2019.

[10] H. A. González, E. Ibarra, P. C. Garcia, and A. C. Victorino, "Quaternion based control for circular UAV trajectory tracking, following a ground vehicle: Real-time," in *20th International Federation of Automatic Control World Congress (IFAC WC)*, vol. 50, 2017.

[11] Y. Hayashi, D. Yashiro, K. Yubai, and S. Komada, "Experimental Validation of Contact Force Control of Quadrotor Based on Rotor Angular Acceleration Control," in *IEEE International Conference on Mechatronics (ICM)*, 2019.

[12] M. Poot, J. Portegies, N. Mooren, M. van Haren, M. van Meer, and T. Oomen, "Gaussian Processes for Advanced Motion Control," *IEEJ Journal of Industry Applications*, vol. 11, no. 3, pp. 396–407, 2022.

[13] X. Zhang, G. Liu, Y. Wu, and N. Sun, "Feedforward Control for Pneumatic Artificial Muscles With Creep Compensation Using Rate-Dependent and Load-Dependent Models," *IEEJ Journal of Industry Applications*, vol. 12, no. 5, pp. 868–875, 2023.

[14] J. Shin, H. Jin Kim, Y. Kim, and W. E. Dixon, "Autonomous Flight of the Rotorcraft-Based UAV Using RISE Feedback and NN Feedforward Terms," *IEEE Transactions of Control Systems Technology*, vol. 20, no. 5, pp. 1392–1399, 2012.

[15] H. Chu, Q. Jing, Z. Chang, Y. Shao, X. Zhang, and M. Mukherjee, "Quadrotor Attitude Control via Feedforward All-Coefficient Adaptive Theory," *IEEE Access*, vol. 8, pp. 116 441–116 453, 2020.

[16] T. Imura, *Wireless Power Transfer Using Magnetic and Electric Resonance Coupling Techniques*. Springer Nature, 2020.

[17] K. Fujimoto, K. Yokota, S. Nagai, and H. Fujimoto, "Modeling and Verification of Pitch-Dependent Coupling Coefficient for WPT to Flying Drone," in *IEE-Japan Industry Applications Society Conference (JIASC)*, 2021.